# Operando direct observation of filament formation in resistive switching devices enabled by a topological transformation molecule

Hou, Kunqi; Chen, Shuai; Zhou, Cheng; Nguyen, Linh Lan; Dananjaya, Putu Andhita; Duchamp, Martial; Bazan, Guillermo C.; Lew, Wen Siang; Leong, Wei Lin

2021

Hou, K., Chen, S., Zhou, C., Nguyen, L. L., Dananjaya, P. A., Duchamp, M., Bazan, G. C., Lew, W. S. & Leong, W. L. (2021). Operando direct observation of filament formation in resistive switching devices enabled by a topological transformation molecule. Nano Letters, 21(21), 9262-9269. https://dx.doi.org/10.1021/acs.nanolett.1c03180

https://hdl.handle.net/10356/153464

https://doi.org/10.1021/acs.nanolett.1c03180

# Operando Direct Observation of Filament Formation in Resistive Switching Devices Enabled by a Topological Transformation Molecule

Kunqi Hou[1], Shuai Chen[2], Cheng Zhou[3], Linh Lan Nguyen[4], Putu Andhita Dananjaya[1], Martial Duchamp[4], Guillermo C. Bazan[3], Wen Siang Lew[1*] and Wei Lin Leong[2*]

[1]*School of Physical and Mathematical Sciences, Nanyang Technological University 21 Nanyang Link, 637371 Singapore.*

[2]*School of Electrical and Electronic Engineering, Nanyang Technological University 50 Nanyang Avenue, 639798 Singapore.*

[3]*Depertment of Chemistry, National University of Singapore 3 Science Drive 3, 117543 Singapore*

[4]*School of Materials Science & Engineering, Nanyang Technological University 50 Nanyang Avenue, 639798 Singapore*

**Corresponding Authors**

***Wei Lin Leong*** *- School of Electrical and Electronic Engineering, Nanyang Technological University 50 Nanyang Avenue, 639798 Singapore. E-mail: wlleong@ntu.edu.sg*

***Wen Siang Lew*** *- School of Physical and Mathematical Sciences, Nanyang Technological University 21 Nanyang Link, 637371 Singapore. E-mail: wensiang@ntu.edu.sg*

**Abstract:** Conductive filaments (CFs) play a critical role in the mechanism of resistive random-access memory (ReRAM) devices. However, in-situ detection and visualization of the precise location of CFs are still key challenges. We demonstrate for the first time, the use of a π-conjugated molecule which can transform between its twisted and planar states upon localized Joule heating generated within filament regions, thus reflecting the locations of the underlying CFs. Customized patterns of CFs were induced and observed by the π-conjugated molecule layer, which confirmed the hypothesis. Additionally, statistical studies on filaments distribution were conducted to study the effect of device sizes and bottom electrode heights, which serves to enhance the understanding of switching behavior and their variability at device level. Therefore, this approach serves great potential in aiding the development of ReRAM technology.

**Keywords:** ReRAM, π-conjugated molecule, conductive filament location, spatial mapping, finite element modeling

Resistive random access memory (ReRAM) is an emerging non-volatile memory technology which is of great interest for embedded device applications such as the internet of things (IoT), automobile and infotainment platforms, as well as neuromorphic computing,[1-6] In comparison to flash memory, ReRAM has the advantages of lower power consumption, and higher operating speed. It also has low cost-per-bit and superior scaling capability.[7, 8] The filamentary model has been widely accepted in explaining the switching process, i.e. formation and rupture of conductive filaments (CFs) within a cell that is typically composed of an insulating oxide layer.[9, 10] The CF is composed of oxygen vacancies or defects generated within the oxide layer when under a voltage bias. The key challenges for wafer-level ReRAM have been the variability in device and array level due to the challenges in large area deposition of high-quality oxides, as well as the random electroforming process.[11, 12]

Locating the CFs is important as it relates directly to the origin of oxygen vacancies and variabilities in switching.[13,14] Conductive-atomic force microscopy (C-AFM) technique has been used to localize the CF on the scanned current map after forming process.[15-21] In-situ transmission electron microscopy (STEM) technique has also been developed to learn the dynamics of defects generation and filament formation.[15, 22] While these characterization techniques provide important information about the physics of the CF in nanoscale region, there are limitations such as the need for removal of top electrode and expertise in specimen preparation, or the use of specimen thinness which can produce an unrealistically small thermal conductance to ambient temperature and alter the switching mechanism,[23] as well as not suitable for large area spatial filament mapping.[23] Direct observation and correlation between CF formation and its electrical behavior during repeated switching in real device operation remains elusive.

In resistive switching, several hundred degrees Celsius within the formed filament region can be reached due to the significant Joule heating effect.[13, 24-27] Based on such temperature effect, an infrared microscopy to detect the existence of filamentary conduction was reported by M. Uenuma, et al. [28,29] The main challenge of this infrared microscopy technique is the calibration of its signal to device temperature and the heat

spreading across the top electrode which could limit its spatial resolution.[29] Another filament detecting method is by spin-coating a photoresist layer over the top electrode, in which the photoresist layer will be burned out at the filament region due to the Joule heating effect, hence, indicating the filament position.[30] However, the burnt-out of the photoresist is permanent, and repeated observations of the filament formation during the reversible switching process cannot be carried out.

Herein, we introduce a simple-yet-effective approach to observe the filament formation in ReRAM device by utilizing an organic π-conjugated molecule, namely, (7,7'-(3,3'-dihexyl-[2,2'-bithiophene]-5,5'-diyl)bis(6-fluoro-4-(5-hexylthiophen-2-yl)benzo[c][1,2,5] thiadiazole)), referred to as "TT", which exhibits a topological transformation with temperature. As shown in **Figure 1a**, the TT molecule contains a flexible bithiophene central fragment, and possesses unique phase transition properties. It presents the amorphous or twisted state in the initial film formation (red color) and can crystallize over time and ultimately adopting a planar configuration (dark blue color)[31, 32]; **Figure 1b**. Grazing incidence wide-angle X-ray scattering (GIWAXS) measurements to support the morphology change have also been reported in previous work.[33] Interestingly, the structural change of the TT film is reversible. Upon heating above 120 °C, the color of TT film changes back to red (amorphous) and to dark blue once the molecule crystallizes over time. At room temperature, this color change of the film took over a period of ~23 minutes. The detailed absorption spectra and color change during the film transition are also shown in Figure S1 and Video 1 of Supporting information respectively. **Figure 1c-d** presents the schematic illustration of the working principle of this work and the optical images of the fabricated cross-point ReRAM device, where the TT molecule film is placed on top of the top electrode (TE) of the ReRAM device. The CFs can be observed and visualized by TT molecule during the switching process since Joule heating at CF region induced the change of structural properties of TT molecule and therefore color change of the TT film. **Figure 1e** shows a representative optical image using this technique, where the location of a conductive filament (red-color spot) is reflected in the optical image at 40 μm×40 μm device after the electrical setting process.

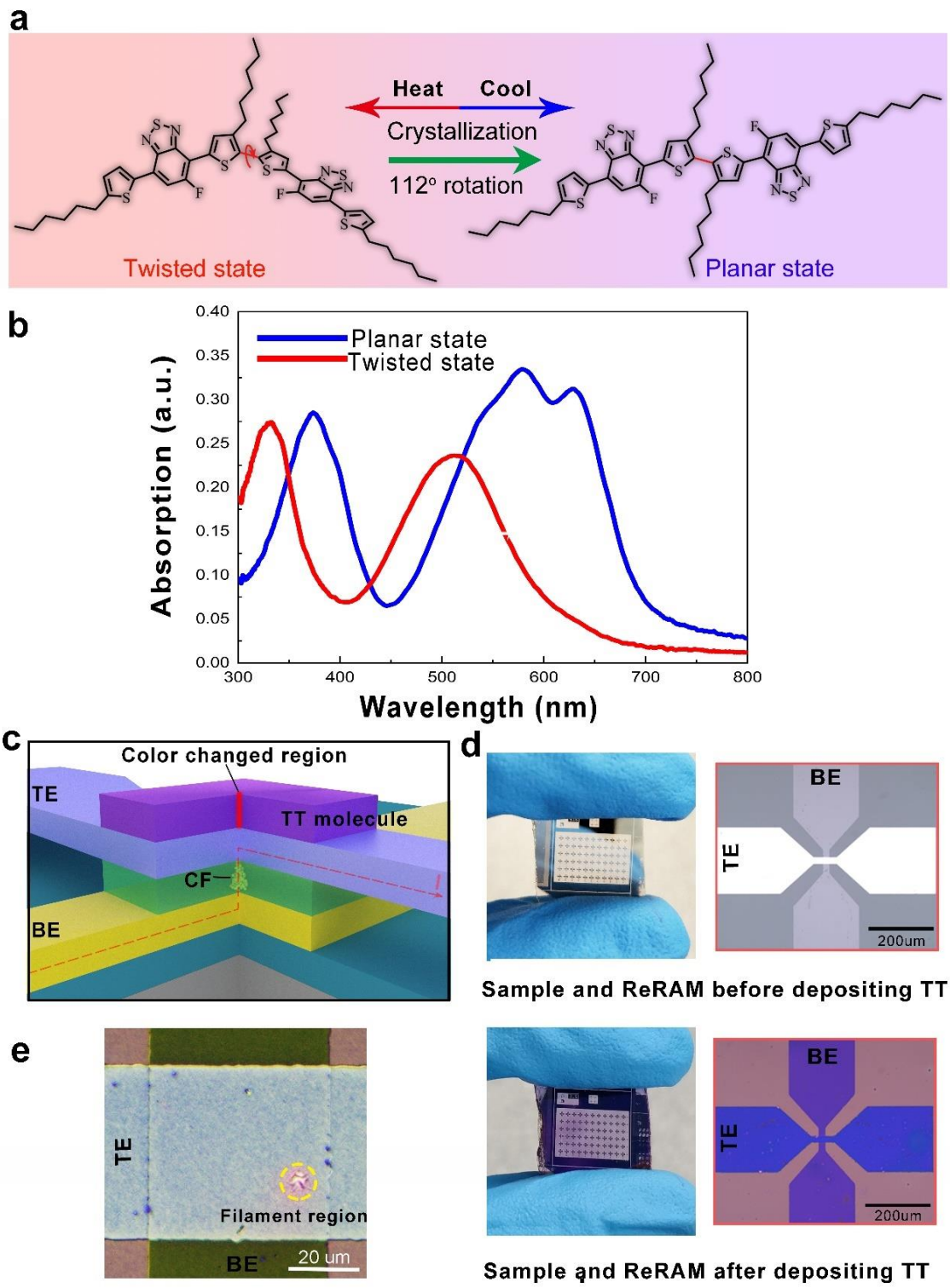


**Figure 1** a) The molecular structure of the TT molecule in the twisted state (left) and the planar state (right). b) UV-vis absorption spectra of the TT film in the twisted (red) and the planar (blue) state. The peak shift from 335nm and 520nm to 375nm and 580nm respectively. c) Schematic demonstration of the working principle of this study. d) Optical images of the fabricated sample and ReRAM device before and after coating of the TT molecule layer. The ReRAM device has a cross-point structure, with a bottom electrode (BE), oxide layer, and top electrode (TE). e) Formation of conductive filament after switching on and the impact of generated Joule heating on the color of π-conjugated molecule layer.

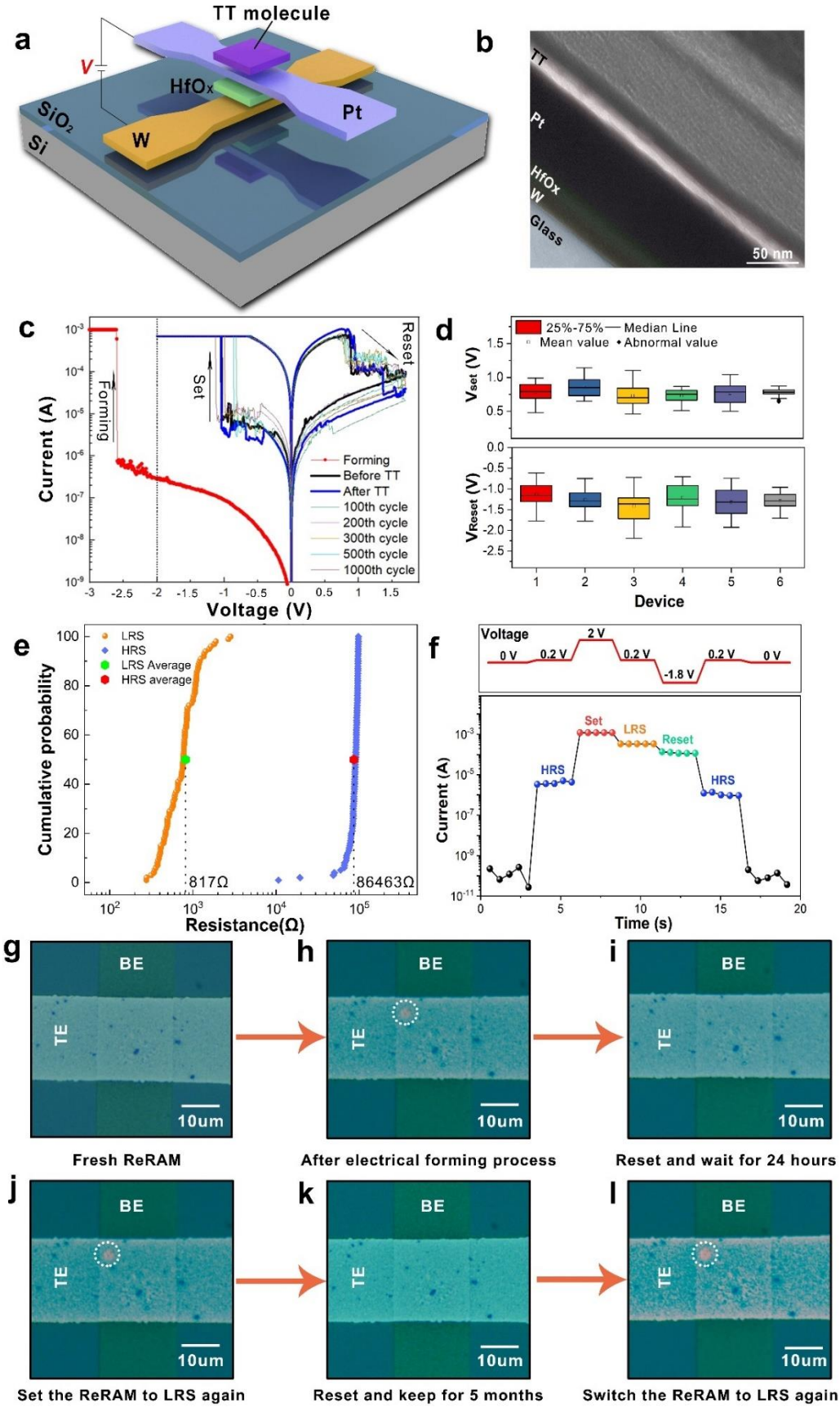


**Figure 2** a) Schematic drawing of ReRAM coated with filament-detection layer. The ReRAM structure of this work is (Tungsten (10nm) - Hafnium oxide (10nm) – Platinum (10nm)) cross-point structure. b)

Cross-section TEM image of the stacked layers in ReRAM. c) The I-V curves of forming, before, and after spin-coating TT film of the ReRAM stack, and the $100^{th}$, $300^{th}$, $500^{th}$, $1000^{th}$ I-V data for the same device after depositing TT molecule with the reset stop voltage of 2V under 1mA compliance current condition. d) The distribution of set and reset voltages of ReRAM device. e) Cumulative probability graph of HRS and LRS among 128×6 DC cycles with a -0.2V read voltage. f) The current waveform during the setting and resetting process, and the current value during the reading process when the device is in LRS and HRS with a 0.2V read voltage. g-l) Optical images of the ReRAM with the device area of 20μm×20μm, which took by 100× microscope. The red spots circled by the dashed lines in the images indicate the approximate locations of the CF, which disappear after the TT film transform to the planar state and reappear again during the setting process after 1 day and 5 months.

The ReRAM device used in this work is Tungsten (10nm) – Hafnium oxide (10nm) – Platinum (10nm)) cross-point structure (**Figure 2a-b**). Hafnium oxide ($HfO_x$) is chosen in this study as it is one of the most commonly used oxide materials for ReRAM devices and the filamentary switching nature has been well-studied.[19, 34-37] The working principle of such ReRAM stack is demonstrated in Figure S2. We first measured the current-voltage (I-V) curves for the ReRAM devices before and after depositing the TT molecule, to ensure that the TT molecule layer does not affect the performance of resistive switching. The tungsten bottom electrode (BE) was grounded, while the voltage bias was applied to the platinum top electrode (TE). As shown in **Figure 2c**, the I-V curves of the devices with and without the TT molecule are similar. We also tested six ReRAM devices containing the TT layers for 128 DC cycles. **Figure 2d** shows the average set and reset voltage for each device. This ReRAM stack gives an average forming, set, and reset voltage of -2.08V, -1.1V, and 0.85V respectively. The resistance of High Resistance State (HRS) and Low Resistance State (LRS) in each cycle were reviewed on I-V curves at -0.2 V. **Figure 2e** shows the cumulative probability of resistance states with 86463 Ω average HRS, and 817 Ω average LRS, yielding an average on-off ratio of ~106. The current dynamics of the ReRAM stack with read-set pulse-read-reset pulse-read waveform are also presented in **Figure 2f**. Good endurance (> 1000 cycles) and fast transient response (< 20 μs) of the ReRAM stack are observed (Figure S3). The ReRAM devices therefore showed stable resistive switching according to these electrical characterization results.

To observe the role of the TT molecule, we first compared the optical images of a

20 μm×20 μm ReRAM device before and after the electrical forming process (**Figure 2g and h**). The red spot circled by the dashed line in **Figure 2h** indicates the approximate location of the CF after the electrical forming process. The red spot gradually disappear once the TT film transformed to planar state (after around 1 day); see **Figure 2i**. We next switched the device to LRS again and the CF is reflected at the same spot location (**Figure 2j**). This is most like due to the secondary formed CF growing from the tip of the previous partially ruptured CF, which has also been reported by previous studies.[38, 39] The reset processes can be done repeatedly even after 5 months (**Figure 2k-l**), which indicates that the partially ruptured CF remains in the oxide layer and the fabricated ReRAM device has good data retention. The color-changing spot appears from a small point and expands quickly to a larger size in hundreds of milli-second because of the heat diffusion (see attached Videos 2 and 3, Supporting information). We note that the recovering time, i.e. the time for the red spot to disappear, can vary from around 12 hours to 1 day. This is due to the generation of different sizes of CFs and therefore varying sizes of the color-changing spots (Figure S4). All filaments formed in different locations of ReRAM devices such as TE edge, BE edge, and center can be successfully detected using this approach (Figure S5).

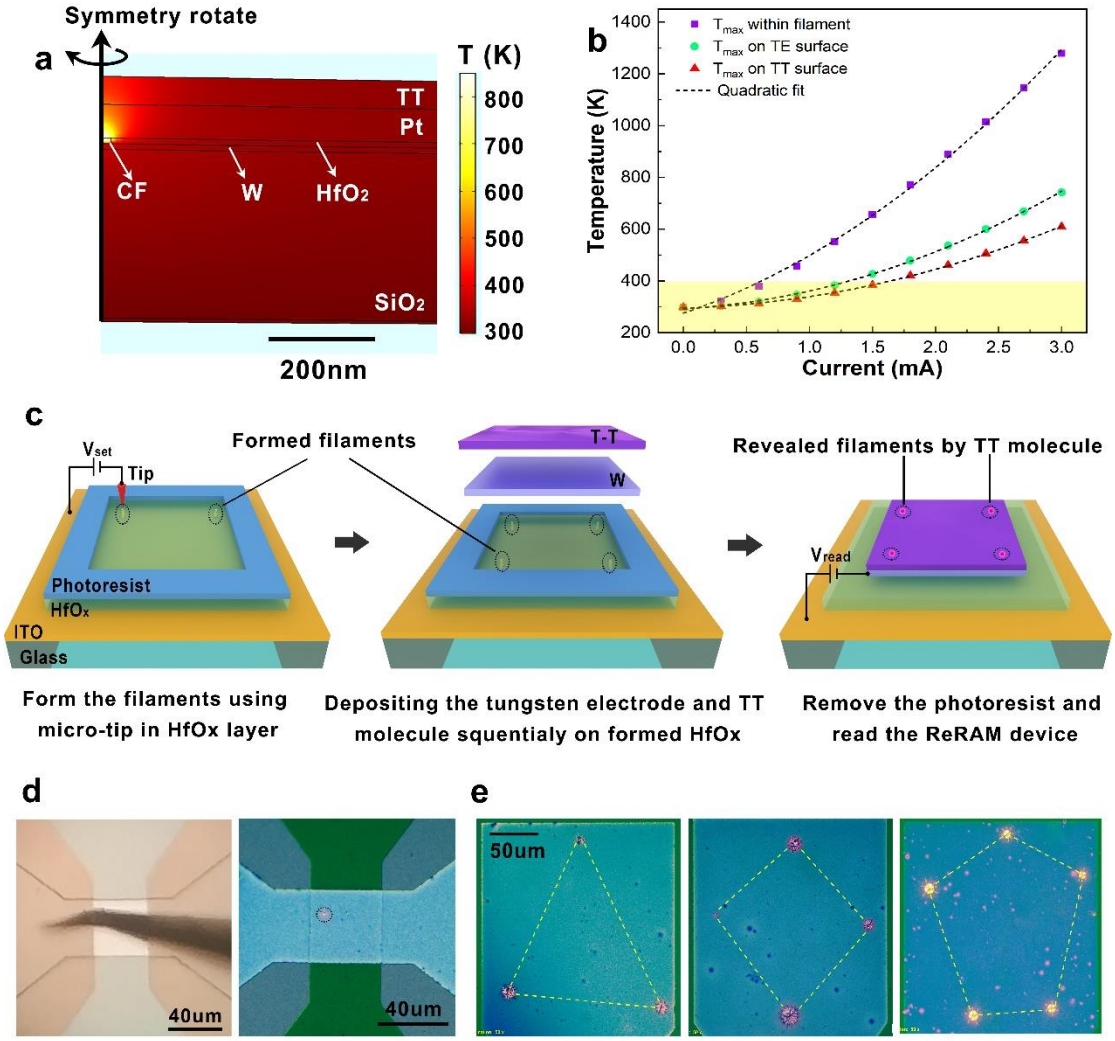


**Figure 3** a) Structure of built 2D axisymmetric ReRAM COMSOL model. b) The maximum temperature value and their fittings of CF (purple), TE surface (green), and TT surface (red) with varying applied current. c) Structure of Indium Tin Oxide substrate (ITO substrate)/$HfO_x$(12nm)/tungsten (the head of micro-tip) ReRAM stack and the operating procedures used in the micro-tip study. d) The optical images of the 40 μm×40 μm ReRAM device during the filament setting and displaying, where the discoloration spots reflect the formed filaments. e) The triangle, diamond, and pentagon pattern created by the tip and reflected by TT film.

The high current density associated with filamentary conduction can cause an increase in temperature due to local Joule heating. A COMSOL model with similar ReRAM device structure was built to further verify the temperature distribution inside the device upon applying the current in LRS. The schematic diagram of the model is shown in **Figure 3a**, where a 2D axisymmetric ReRAM model was built up in COMSOL. The detailed information of varying parameters used inside the model can

be found in the Supplement information (Note 1). The simulated maximum temperature values of CF, TE surface, and TT molecule surface as a function of applied currents were plotted in **Figure 3b**. The temperature (T) displays a quadratic relationship with the applied current (I), where $T \propto P = I^2 \times R$, where P refers to power of Joule heating and R is resistance. The simulations results showed that the temperature on the TT surface can reach 400 K (~127℃) under the condition of 1.6 mA read current, which is sufficient to modulate the topological state of the organic film (~120℃). The simulation studies on varying CF sizes and TE thicknesses, as well as temperature diffusion dynamics were also conducted, which are shown in Figure S6. The simulation results therefore give qualitatively proof of the proposed method, where the Joule heating generated can be used to optically modulate the TT film.

To further verify this new filament detection method, we carried filaments programming through a micro-tip before the deposition of the TT molecule. A tungsten micro-tip with ~5 μm diameter was placed in direct contact with the $HfO_x$ film, which was deposited on indium tin oxide (ITO) substrate. The ITO and the tungsten tip serve as BE and TE respectively. The CFs can therefore be formed within the oxide layer by applying the voltage bias through the tip and ITO substrate. (Figure S7) Thereafter, varying numbers of CFs could be formed in different locations. The tungsten tip is then removed, and the platinum TE and TT film were deposited sequentially. A read voltage is then applied to the ReRAM stack. The schematic diagram of this process is shown in **Figure 3c**. As presented in **Figure 3d**, the filament that is pre-set by the tungsten tip is reflected by the spot of color change on TT film. We also created more customized filaments using the micro-tip, where the formed filaments are in shapes of triangle, diamond, and pentagon, and all these formed filaments were reflected by TT film accurately (**Figure 3e**). Hence, this filament programming study gives quantitative confirmation of such filament detection method.

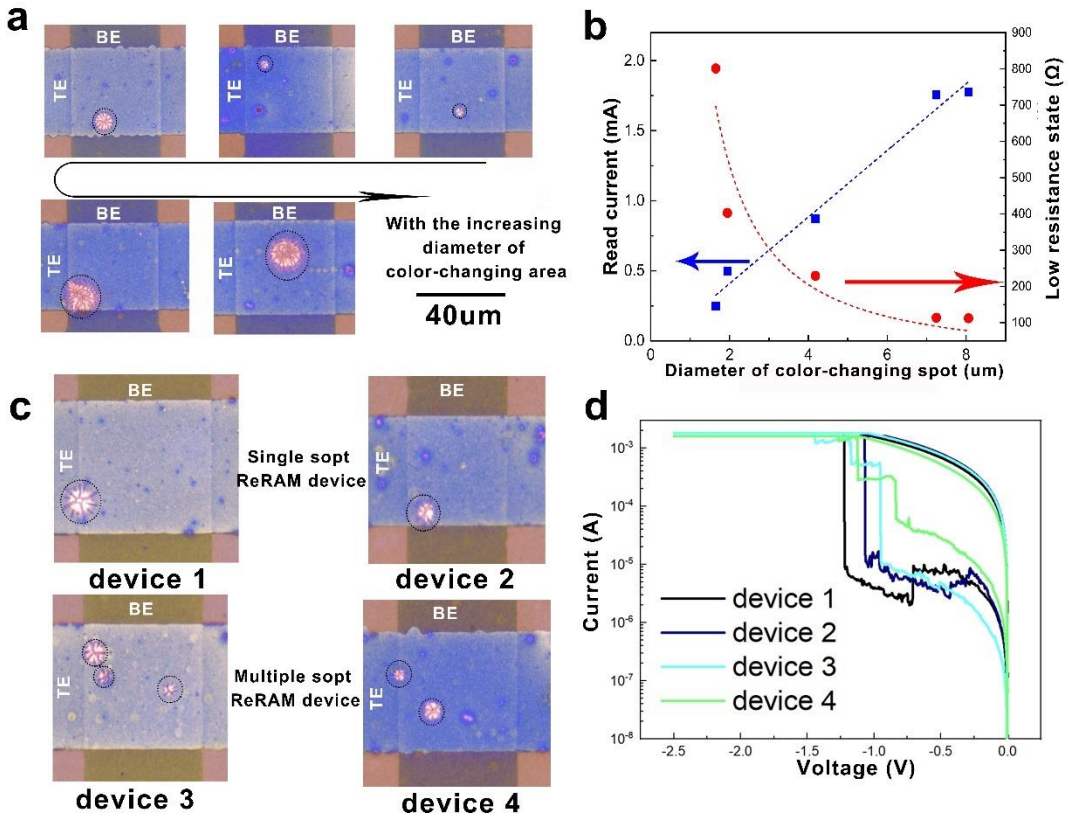


**Figure 4** a) Optical images of 5 ReRAMs with varying color spot size. b) The relationship between the color spot size and the read current value (blue), and resistance value in LRS (red). c) Optical images of ReRAMs with different spot numbers. d) The relationship between spot numbers and the shape of the I-V curve during the forming process.

Besides the position, the size of formed CFs can also be monitored by the TT film, where a larger color spot larger indicates a larger size of CF due to the larger heat diffusion area (**Figure 4a**). We further correlate these different sizes of CFs with the resistance and read current values in LRS, where the resistance value decreases as the color spot size increases, and the read current (under a 0.2 V read voltage) showed a positive relationship with the color spot size (**Figure 4b)**, in agreement with previous studies.[40] Moreover, in some other devices, multiple color spots can be observed which indicates that more filaments were generated during the forming cycle. As shown in **Figure 4c-d**, multiple increment steps (resistance states) can be observed in the I-V curves for multiple CF-based ReRAMs (device 3 and 4), while the current value directly reached the compliance for single CF-based ReRAMs (device 1 and 2).

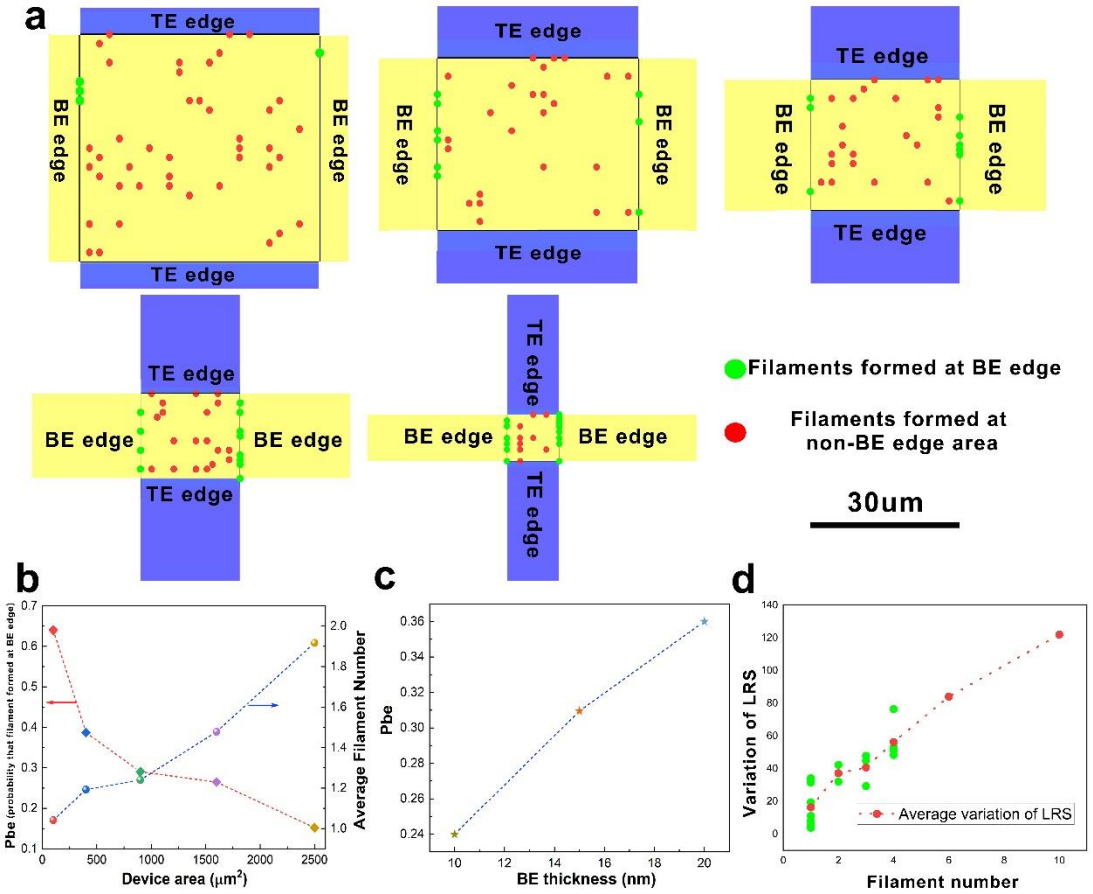


**Figure 5** a) The spatial maps of the CF distribution for 10 μm×10 μm to 50 μm×50 μm ReRAMs. b) The statistical result on the CF number per device and $P_{be}$, and their relationship to the device area. c) The value of $P_{be}$ with respect to BE thickness. 40 ReRAM devices were measured for each BE thickness. d) The variations of LRS in 32DC cycles for 18 ReRAM devices, and its relationship with the CF number.

We further conduct a statistical study, which focuses on the spatial distribution of CFs to understand the relationship between filament-forming and ReRAM device geometry. Here, a total of 200 devices were fabricated with varying sizes (from 10 μm×10 μm to 50 μm×50 μm) and BE thicknesses (10 nm, 15 nm, and 20 nm). The location of CFs for each device was recorded through the color-changing spot of TT film after the electro-forming process. The detailed information on the procedure to obtain the filament coordinates is shown in Figure S8. **Figure 5a** shows the spatial mappings of the CF distribution with varying sizes (BE height was kept at 10nm). In general, there is a trend that more filaments tend to be formed for larger-area devices (**Figure 5b**). In addition, the number of CFs formed at the edge of BE is found to

increase significantly with decreasing device size. The probability of filament forming at BE edge ($P_{be}$) also displayed an inverse proportion to the device size (**Figure 5b**). We postulate that this is likely due to the device fabrication process where the BEs were directly deposited on substrates. This will cause edge effect, where the thickness of deposited oxide film is not uniform and will induce thinner oxide thickness at the edge area of BE. This edge effect is also more pronounced with higher BE thickness,[30, 41] where increasing number of CFs are formed at the BE edge (~24%, ~31% and ~36%) for increasing BE thickness (10 nm, 15 nm, and 20 nm); **Figure 5c**.

Multiple filaments based ReRAM are typically not desired as the setting process might not switch on every filament which will induce a larger uncertainty in LRS. Using this approach, we also compared the performance of ReRAM devices with varying number of filaments. 18 devices with varying filament numbers were conducted for 32 DC cycles. The variations in HRS and LRS were extracted from the cycling data. As shown in **Figure 5d**, single filament based ReRAM is shown to exhibit a more stable resistance state in LRS. The average variation in LRS for single-filament ReRAM is less than 20%, and the variation is found to increase with increasing filament numbers. The variations of HRS, set voltage, and reset voltage among these devices were also summarized in the supporting information (Figure S9-11). Our results indicate that scaling down the device size is a way to control the filament number and minimize the variations.

In conclusion, an operando direct observation of filament formation and its properties for ReRAM at device level has been enabled by using a thermoresponsive conjugated molecule. The number, size, and position of CFs that formed within the oxide layer are revealed by the localized color change of the π-conjugated molecule layer. Such method expands the filaments in nanoscale to micro-scale by color-changing spots, which were formed by the diffusion of localized Joule heating. Most importantly, the location can be easily observed and studied using a simple optical microscope. Notably, this organic molecule can display the CFs repeatably, which revealed the same filament multiple times over 5 months period interval. A 2D axisymmetric ReRAM model has been built up to confirm this filament positioning

method, where the results showed that the temperature increment generated by the Joule heating effect can induce the structural transformation of the organic film. CFs were also deliberately programmed by the micro-tip, and the TT film was able to reflect the same CF locations, which confirms the viability of this approach. Finally, using this approach, we found that (1) multiple CFs are relatively easier to form in devices with larger area, (2) there is a higher possibility of CFs formation at the edge of BE with decreasing device size and increasing BE thickness, and (3) the variations in LRS for single filament devices were smaller. The resolution of this filament detection method can be further improved by limiting the amount of heat generation, which requires an accurate current limiter, e.g., transistor. If the amount of current/heat could be precisely controlled, the color-changing area will be confined to a smaller region. We believe the filament positioning method based on the topological transformation of TT molecule is a powerful technique to study filament properties and design of high-performing ReRAM devices.

## Experimental section

Experimental details on ReRAM device fabrication, electrical characterization, TT film preparation, and TEM sample preparation are shown in Note 2 and 3 (Supplement document)

## Supporting Information

Methods and experimental details, absorption spectra during the transition of the TT film, heightmap of ReRAM device area characterized by AFM, endurance data, transient response during set process and reset process for fabricated ReRAM, COMSOL simulation results, optical images of color-changing spots I-V curves for filament programming, variations of HRS, set voltage, and reset voltage.

Video 1 (Color-changing video of TT film heated on 125° hotplate)

Video 2 (Formation and expansion of color-changing spot)

Video 3 (Formation and expansion of color-changing spot)

## Acknowledgments

The authors would like to acknowledge funding support from A*STAR AME IAF-ICP Grant (No. I1801E0030) grant. This work is also supported by Ministry of Education (MOE) under AcRF Tier 2 grant (2019-T2-2-106) and National Robotics Programme (W1925d0106).

## Reference


1. Yu, S., Resistive random access memory (RRAM). *Synthesis Lectures on Emerging Engineering Technologies* **2016,** *2* (5), 1-79.
2. Chen, Y., ReRAM: History, Status, and Future. *IEEE Transactions on Electron Devices* **2020,** *67* (4), 1420-1433.
3. Lim, E. W.; Ismail, R., Conduction mechanism of valence change resistive switching memory: a survey. *Electronics* **2015,** *4* (3), 586-613.
4. Lanza, M.; Wong, H. S. P.; Pop, E.; Ielmini, D.; Strukov, D.; Regan, B. C.; Larcher, L.; Villena, M. A.; Yang, J. J.; Goux, L., Recommended methods to study resistive switching devices. *Advanced Electronic Materials* **2019,** *5* (1), 1800143.
5. Hong, X.; Loy, D. J.; Dananjaya, P. A.; Tan, F.; Ng, C.; Lew, W., Oxide-based RRAM materials for neuromorphic computing. *Journal of materials science* **2018,** *53* (12), 8720-8746.
6. Prabhu, N. L.; Loy Jia Jun, D.; Dananjaya, P. A.; Lew, W. S.; Toh, E. H.; Raghavan, N., Exploring the Impact of Variability in Resistance Distributions of RRAM on the Prediction Accuracy of Deep Learning Neural Networks. *Electronics* **2020,** *9* (3), 414.
7. Wei, Z.; Kanzawa, Y.; Arita, K.; Katoh, Y.; Kawai, K.; Muraoka, S.; Mitani, S.; Fujii, S.; Katayama, K.; Iijima, M. In *Highly reliable TaOx ReRAM and direct evidence of redox reaction mechanism*, 2008 IEEE International Electron Devices Meeting, IEEE: 2008; pp 1-4.
8. Lee, M.-J.; Lee, C. B.; Lee, D.; Lee, S. R.; Chang, M.; Hur, J. H.; Kim, Y.-B.; Kim, C.-J.; Seo, D. H.; Seo, S., A fast, high-endurance and scalable non-volatile memory device made from asymmetric Ta 2 O 5− x/TaO 2− x bilayer structures. *Nature materials* **2011,** *10* (8), 625-630.
9. Russo, U.; Ielmini, D.; Cagli, C.; Lacaita, A. L., Filament conduction and reset mechanism in NiO-based resistive-switching memory (RRAM) devices. *IEEE Transactions on Electron Devices* **2009,** *56* (2), 186-192.
10. Privitera, S.; Bersuker, G.; Butcher, B.; Kalantarian, A.; Lombardo, S.; Bongiorno, C.; Geer, R.; Gilmer, D.; Kirsch, P., Microscopy study of the conductive filament in HfO2 resistive switching memory devices. *Microelectronic Engineering* **2013,** *109*, 75-78.
11. Chen, A.; Lin, M.-R. In *Variability of resistive switching memories and its impact on crossbar array performance*, 2011 International Reliability Physics Symposium, IEEE: 2011; pp MY. 7.1-MY. 7.4.
12. Fantini, A.; Goux, L.; Degraeve, R.; Wouters, D.; Raghavan, N.; Kar, G.; Belmonte, A.; Chen, Y.-Y.; Govoreanu, B.; Jurczak, M. In *Intrinsic switching variability in HfO 2 RRAM*, 2013 5th IEEE International Memory Workshop, IEEE: 2013; pp 30-33.
13. Guan, X.; Yu, S.; Wong, H.-S. P., On the switching parameter variation of metal-oxide RRAM—Part I: Physical modeling and simulation methodology. *IEEE Transactions on electron devices* **2012,** *59* (4), 1172-1182.

14. Yang, H.; Wang, Z.; Guo, X.; Su, H.; Sun, K.; Yang, D.; Xiao, W.; Wang, Q.; He, D., Controlled Growth of Fine Multifilaments in Polymer-Based Memristive Devices Via the Conduction Control. *ACS Applied Materials & Interfaces* **2020,** *12* (30), 34370-34377.
15. Celano, U.; Yin Chen, Y.; Wouters, D. J.; Groeseneken, G.; Jurczak, M.; Vandervorst, W., Filament observation in metal-oxide resistive switching devices. *Applied Physics Letters* **2013,** *102* (12), 121602.
16. Ranjan, A.; Pey, K.; O'Shea, S., The interplay between drift and electrical measurement in conduction atomic force microscopy. *Review of Scientific Instruments* **2019,** *90* (7), 073701.
17. Niu, G.; Calka, P.; der Maur, M. A.; Santoni, F.; Guha, S.; Fraschke, M.; Hamoumou, P.; Gautier, B.; Perez, E.; Walczyk, C., Geometric conductive filament confinement by nanotips for resistive switching of HfO 2-RRAM devices with high performance. *Scientific reports* **2016,** *6* (1), 1-9.
18. Buckwell, M.; Montesi, L.; Hudziak, S.; Mehonic, A.; Kenyon, A. J., Conductance tomography of conductive filaments in intrinsic silicon-rich silica RRAM. *Nanoscale* **2015,** *7* (43), 18030-18035.
19. Lanza, M., A review on resistive switching in high-k dielectrics: A nanoscale point of view using conductive atomic force microscope. *Materials* **2014,** *7* (3), 2155-2182.
20. Son, J.; Shin, Y.-H., Direct observation of conducting filaments on resistive switching of NiO thin films. *Applied Physics Letters* **2008,** *92* (22), 222106.
21. Nardi, F.; Deleruyelle, D.; Spiga, S.; Muller, C.; Bouteille, B.; Ielmini, D., Switching of nanosized filaments in NiO by conductive atomic force microscopy. *Journal of Applied Physics* **2012,** *112* (6), 064310.
22. Kwon, D.-H.; Kim, K. M.; Jang, J. H.; Jeon, J. M.; Lee, M. H.; Kim, G. H.; Li, X.-S.; Park, G.-S.; Lee, B.; Han, S., Atomic structure of conducting nanofilaments in TiO 2 resistive switching memory. *Nature nanotechnology* **2010,** *5* (2), 148-153.
23. Walczyk, C.; Walczyk, D.; Schroeder, T.; Bertaud, T.; Sowinska, M.; Lukosius, M.; Fraschke, M.; Wolansky, D.; Tillack, B.; Miranda, E., Impact of Temperature on the Resistive Switching Behavior of Embedded $HfO_x$-Based RRAM Devices. *IEEE transactions on electron devices* **2011,** *58* (9), 3124-3131.
24. Sato, Y.; Kinoshita, K.; Aoki, M.; Sugiyama, Y., Consideration of switching mechanism of binary metal oxide resistive junctions using a thermal reaction model. *Applied physics letters* **2007,** *90* (3), 033503.
25. Chang, S.; Chae, S.; Lee, S.; Liu, C.; Noh, T.; Lee, J.; Kahng, B.; Jang, J.; Kim, M.; Kim, D.-W., Effects of heat dissipation on unipolar resistance switching in Pt/ Ni O/ Pt capacitors. *Applied Physics Letters* **2008,** *92* (18), 183507.
26. Larcher, L.; Padovani, A.; Pirrotta, O.; Vandelli, L.; Bersuker, G. In *Microscopic understanding and modeling of HfO 2 RRAM device physics*, 2012 International Electron Devices Meeting, IEEE: 2012; pp 20.1. 1-20.1. 4.
27. Puglisi, F. M.; Larcher, L.; Padovani, A.; Pavan, P., Bipolar Resistive RAM Based on $HfO_x$: Physics, Compact Modeling, and Variability Control. *IEEE Journal on Emerging and Selected Topics in Circuits and Systems* **2016,** *6* (2), 171-184.
28. Uenuma, M.; Ishikawa, Y.; Uraoka, Y., Joule heating effect in nonpolar and bipolar

resistive random access memory. *Applied Physics Letters* **2015,** *107* (7), 073503.
29. Massey, G. A.; Davis, J. A.; Katnik, S.; Omon, E., Subwavelength resolution far-infrared microscopy. *Applied optics* **1985,** *24* (10), 1498-1501.
30. Nath, S. K.; Nandi, S. K.; Li, S.; Elliman, R. G., Detection and spatial mapping of conductive filaments in metal/oxide/metal cross-point devices using a thin photoresist layer. *Applied Physics Letters* **2019,** *114* (6), 062901.
31. Seifrid, M. T.; Reddy, G. M.; Zhou, C.; Chmelka, B. F.; Bazan, G. C., Direct Observation of the Relationship between Molecular Topology and Bulk Morphology for a π-Conjugated Material. *Journal of the American Chemical Society* **2019,** *141* (13), 5078-5082.
32. Wedler, S.; Zhou, C.; Bazan, G. C.; Panzer, F.; Köhler, A., Role of Torsional Flexibility in the Film Formation Process in Two π-Conjugated Model Oligomers. *The Journal of Physical Chemistry Letters* **2020,** *11* (21), 9379-9386.
33. Zhou, C.; Cui, Q.; McDowell, C.; Seifrid, M.; Chen, X.; Brédas, J. L.; Wang, M.; Huang, F.; Bazan, G. C., Topological Transformation of π-Conjugated Molecules Reduces Resistance to Crystallization. *Angewandte Chemie* **2017,** *129* (32), 9446-9449.
34. Liu, C.-F.; Tang, X.-G.; Wang, L.-Q.; Tang, H.; Jiang, Y.-P.; Liu, Q.-X.; Li, W.-H.; Tang, Z.-H., Resistive switching characteristics of HfO2 thin films on mica substrates prepared by Sol-Gel process. *Nanomaterials* **2019,** *9* (8), 1124.
35. PhilipáWong, H.-S., Multi-level control of conductive nano-filament evolution in HfO 2 ReRAM by pulse-train operations. *Nanoscale* **2014,** *6* (11), 5698-5702.
36. Cartoixà, X.; Rurali, R.; Suñé, J., Transport properties of oxygen vacancy filaments in metal/crystalline or amorphous HfO 2/metal structures. *Physical Review B* **2012,** *86* (16), 165445.
37. Lee, H.; Chen, P.; Wu, T.; Chen, Y.; Wang, C.; Tzeng, P.; Lin, C.; Chen, F.; Lien, C.; Tsai, M.-J. In *Low power and high speed bipolar switching with a thin reactive Ti buffer layer in robust HfO2 based RRAM*, 2008 IEEE International Electron Devices Meeting, IEEE: 2008; pp 1-4.
38. Huang, P.; Liu, X. Y.; Chen, B.; Li, H. T.; Wang, Y. J.; Deng, Y. X.; Wei, K. L.; Zeng, L.; Gao, B.; Du, G., A physics-based compact model of metal-oxide-based RRAM DC and AC operations. *IEEE transactions on electron devices* **2013,** *60* (12), 4090-4097.
39. Larcher, L.; Puglisi, F. M.; Pavan, P.; Padovani, A.; Vandelli, L.; Bersuker, G., A compact model of program window in HfO x RRAM devices for conductive filament characteristics analysis. *IEEE Transactions on Electron Devices* **2014,** *61* (8), 2668-2673.
40. Nardi, F.; Ielmini, D.; Cagli, C.; Spiga, S.; Fanciulli, M.; Goux, L.; Wouters, D., Control of filament size and reduction of reset current below 10 μA in NiO resistance switching memories. *Solid-State Electronics* **2011,** *58* (1), 42-47.
41. Leroy, J.; Crunteanu, A.; Bessaudou, A.; Cosset, F.; Champeaux, C.; Orlianges, J.-C., High-speed metal-insulator transition in vanadium dioxide films induced by an electrical pulsed voltage over nano-gap electrodes. *Applied Physics Letters* **2012,** *100* (21), 213507.

## TOC Graphic

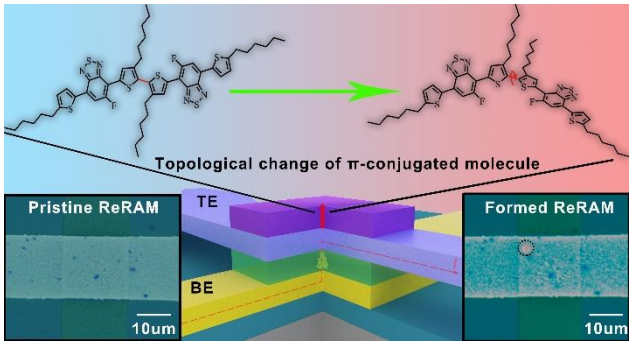
Topological change of π-conjugated molecule
Pristine ReRAM
TE
BE
Formed ReRAM
10um
10um